Inorganic Chemistry

Article

pubs.acs.org/IC

Magnetic Properties and Electronic Structures of Ar_3U^{IV}–L Complexes with Ar = $C_5(CH_3)_4H^-$ or $C_5H_5^-$ and L = CH_3, NO, and Cl

Frédéric Gendron,[†] Boris Le Guennic,*[,‡] and Jochen Autschbach*[,†]

[†]Department of Chemistry, University at Buffalo, State University of New York, Buffalo, New York 14260-3000, United States

[‡]Institut des Sciences Chimiques de Rennes, UMR 6226 CNRS-Université de Rennes 1, 263 Avenue du Général Leclerc, 35042 Rennes Cedex, France

Supporting Information

ABSTRACT: Electronic structures and magnetic properties of the U^{4+} complexes $(C_5Me_4H)_3UNO$, $(C_5Me_4H)_3UCl$, $(C_5H_5)_3UCH_3$, and $(C_5H_5)_3UCl$ are investigated by quantum chemical calculations. On the basis of wave function calculations including spin–orbit (SO) interactions, all complexes have nondegenerate nonmagnetic ground states. However, for L = CH_3 and Cl magnetic doublet excited states are very low in energy, rendering the magnetic susceptibility strongly temperature dependent above ca. 50–100 K. In contrast, $(C_5Me_4H)_3UNO$ exhibits temperature-independent paramagnetism even at room temperature. The calculated susceptibilities agree well with available experimental data. An analysis of the ground states and the magnetic behavior is performed using crystal-field (CF) models with parameters extracted from the ab initio calculations, and with the help of natural orbitals contributing to the electron density, generated from scalar relativistic and SO wave functions for the ground states and selected excited states. Electronic *g*-factors calculated from the CF models agree well with ab initio data. The U–NO bond order in $(C_5Me_4H)_3UNO$ decreases somewhat due to SO coupling, because U–NO bonding π orbitals with strong U $5f_\pi$ character mix with nonbonding $5f_\delta$ orbitals under the SO interaction. This complex also exhibits pronounced multireference character. All complexes afford U-ligand 5f covalent character.

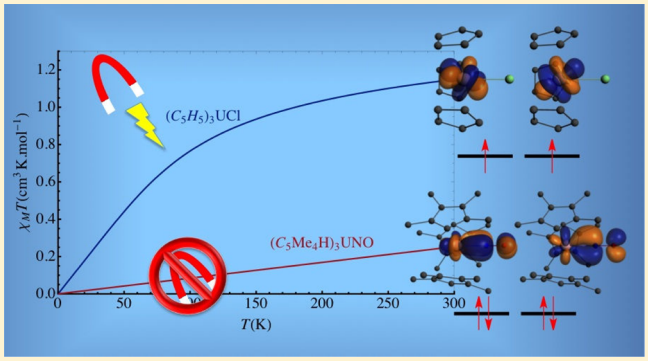

1. INTRODUCTION

Characterizing and rationalizing of the magnetic properties and electronic structures of complexes containing uranium has received considerable attention over the last decades. Compared to lanthanide complexes, the partially covalent 5f character of uranium–ligand bonds and the fact that for the uranium 5f shell the crystal-field (CF) interactions and spin–orbit (SO) coupling can be of comparable magnitudes render the study of these complexes rather challenging.[1−3] Besides being fundamentally interesting in chemistry, the interplay of covalency, CF interactions, and SO coupling may give rise to intriguing magnetic behavior. The latter may be useful, for instance, for single-molecule magnets or spin qubits,[4−9] or to help deducing information about electronic structure and bonding from experimental data. A large amount of experimental magnetic data is available for uranium complexes.[10−13] Despite much progress on the theoretical front, the relationships between molecular structure, chemical bonding, and the observed magnetic properties of uranium and other actinide ions remain insufficiently well-understood.

The magnetic behavior of tetravalent U(IV) $5f^2$ systems is rather interesting. Typically, such U(IV) complexes possess a nondegenerate (singlet) electronic ground state and exhibit temperature (T) independent paramagnetism[14] (TIP) at low T, typically below ca. 50–100 K. At higher T, temperature-dependent paramagnetism is observed. However, Siladke et al. recently synthesized and characterized the U(IV) complex $(C_5Me_4H)_3UNO$ and found TIP even at room temperature.[15] So far this system is the only example of a U $5f^2$ complex that does not exhibit T-dependent paramagnetism at ambient temperatures. For some organo-uranium(IV) complexes it is even possible to acquire NMR spectra which, however, exhibit large paramagnetic effects such as methyl proton shifts on the order of +200 ppm at room temperature for $(C_5H_5)_3UCH_3$.[16]

TIP is caused by magnetic coupling of a nonmagnetic ground state with low-energy excited states, i.e., by nonzero transition matrix elements of the magnetic moment operator (Zeeman operator). The magnitude of the TIP is inversely proportional to the energy difference between the ground state and the excited electronic states. Six decades ago the presence of a "feeble TIP"[17] was used to deduce a covalent participation of uranium 5f orbitals in the U–O bonds of uranyl(VI), UO_2^{2+}. Uranyl(VI) is formally in a $5f^0$ configuration; calculated U charges are around +3. The ground state is closed shell nonmagnetic. Participation of U 5f orbitals in the U–O bonds

Received: September 30, 2014
Published: November 26, 2014

was shown to generate large enough magnetic transition moments to support the magnitude of the TIP of uranyl(VI) found experimentally. For the singlet ground states of U(IV) complexes, magnetic transition moments between states within the 5f manifold can be expected to dominate the TIP. Due to the small excitation energies, TIP is then only observed at low T where thermal population of the excited 5f states is negligible.

The use of quantum chemistry in the understanding of the properties of actinide ions is crucial.[18−20] For example, ab initio quantum chemistry methods as well as semiempirical models based on CF models have been applied successfully to magnetic properties of octahedral $5f^1$ actinide AnR_6 (R = halide, alkyl, alkoxide) and of $5f^3$ An(III) complexes.[1,21−32] In recent studies, we used a combination of complete active space (CAS) multireference wave function methods [self-consistent field (CASSCF)[33] & CASSCF with second-order perturbation theory for dynamic correlation (CASPT2)[34]] and density functional theory (DFT)[35] to investigate the magnetic properties of a series of free actinyl ions (AnO_2^{n+}) and equatorially coordinated actinyl species.[36,37] The CAS calculations allowed us to (i) describe the low-energy part of the electronic spectra properly (i.e., states from the 5f manifold), and (ii) reproduce the observed magnetic properties (electron paramagnetic resonance (EPR) g-factors and in ref 37 also estimates for NMR ligand shifts). Furthermore, a chemically intuitive characterization of the electronic states was made possible with the help of CF models, and with natural orbitals (NOs, see section 2) and natural orbitals for the spin-magnetization ("natural spin orbitals", or NSOs) calculated from the many-electron wave functions including SO coupling.

In the present study we apply a similar computational strategy to investigate the magnetic properties of a set of uranium(IV) complexes, namely, $(C_5Me_4H)_3UCl$, $(C_5H_5)_3UCl$, $(C_5H_5)_3UCH_3$, and $(C_5Me_4H)_3UNO$ (see Figure 1). The

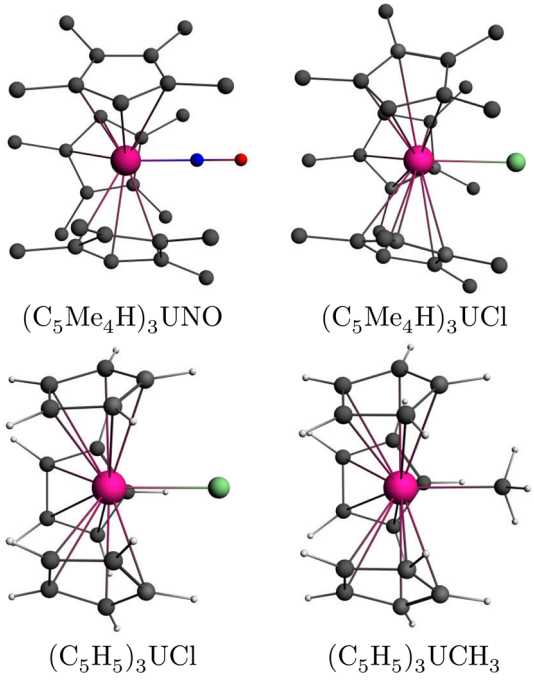

Figure 1. U(IV) complexes studied in this work (optimized structures): purple = U; blue = N; red = O, green = Cl, black = C, gray = H.

magnetic susceptibility of $(C_5H_5)_3UCl$ has been experimentally characterized in the early 1970s.[16,38,39] The magnetic susceptibility was independent of T below 90 K and became paramagnetic at higher temperature. A similar behavior has been found for $(C_5Me_4H)_3UCl$,[15] with TIP below 50 K. The magnetic susceptibilities of such complexes were rationalized with the help of CF theory in the late 1980s by Amberger et al.[40,41] The TIP below 90 K of $(C_5H_5)_3UCl$ was attributed to the effect of the trigonal crystal field which gives rise to a nondegenerate ground state by splitting the 9-fold degeneracy of the $^3H_4$ ground multiplet of the $5f^2$ ion after considering the SO interaction. As discussed in section 3, with scalar relativistic calculations, i.e., excluding SO coupling, the complexes with L = CH_3 and Cl have spin-triplet ground states. Regarding $(C_5Me_4H)_3UNO$, Bursten et al. predicted in 1989 with the help of $X\alpha$ calculations that the closely related system $(C_5H_5)_3UNO$ has a closed shell spin-singlet ground state at the scalar relativistic level.[42] Results from scalar relativistic DFT calculations reported in ref 15 confirmed a spin-singlet ground state. A number of scalar-relativistic DFT studies have been performed on these systems and related complexes.[15,42−44] However, to our knowledge so far no ab initio theoretical investigation of the complexes of Figure 1 has been conducted by taking into account the influence of SO coupling, and the magnetic susceptibilities have not been calculated ab initio.

In the present study, we provide ab initio data for the magnetic susceptibilities, assignments of the low-energy parts of the electronic spectra, as well as characterizations of selected states based on natural orbitals and their occupations and based on CF models. For the ground states, we also compare scalar relativistic and SO CAS calculations with scalar relativistic DFT in order to connect with prior art. At the SO level, for $(C_5H_5)_3UCl$, $(C_5Me_4H)_3UCl$, and $(C_5H_5)_3UCH_3$, zero-field splitting (ZFS) of the scalar spin-triplet ground states, which is caused (predominantly for systems with heavy elements) by the SO interaction, may result in a nondegenerate ground state and a paramagnetic doublet excited state close in energy. The calculated magnetic susceptibilities of $(C_5H_5)_3UCl$, $(C_5Me_4H)_3UCl$, and $(C_5H_5)_3UCH_3$ exhibit the T-dependence that one would expect from the presence or absence of a magnetic excited state at very low energy. However, the scalar relativistic ground state spin-triplets contribute only between 12−40% to the SO ground state wave functions, and the electronic structure is better analyzed after considering SO coupling, via the CF splitting of the J = 4 term of U^{4+}. For $(C_5Me_4H)_3UNO$, SO coupling does not alter the fact that the ground state is nondegenerate, but it has a noticeable influence on the U−NO π bond order. The excited states of this complex are energetically well-separated from the ground state. The TIP of the system is dominated by the second excited state.

Computational and theoretical details are provided in section 2. The results are analyzed and discussed in section 3. A brief summary can be found in section 4.

2. COMPUTATIONAL DETAILS

DFT optimizations of the molecular structures of the complexes in Figure 1 were carried out with the 2013 release of the Amsterdam Density Functional (ADF) package.[45−47] The open metal shells were in some cases treated with fractional orbital occupations resembling an average of electronic configurations. Details can be found in the Supporting Information (SI), Table S1. The structure optimizations utilized the scalar relativistic all-electron zeroth-order regular approximation (ZORA) Hamiltonian,[48] the B3LYP[49] hybrid functional, and a triple-ζ doubly polarized all-electron Slater type basis

dx.doi.org/10.1021/ic502365h | Inorg. Chem. 2014, 53, 13174−13187

Table 1. Comparison of Selected Optimized Distances (Å) and Angles (deg) for $(C_5Me_4H)_3UNO$, $(C_5Me_4H)_3UCl$, $(C_5H_5)_3UCl$, and $(C_5H_5)_3UCH_3$[a]

U−Ar	U−X	Ar−U−Ar	Ar−U−X	state	ΔE (cm^{-1})	ref
$(C_5Me_4H)_3UNO$						
2.561	1.951	119.04	95.67	singlet[b]	0	
(2.491)	(2.013)	(118.8)	(96.5)			15
$(C_5Me_4H)_3UCl$						
2.576	2.639	117.36	99.44	singlet	9679	
2.591	2.648	117.28	99.58	triplet	0	
(2.520)	(2.637)	(117.9)	(98.4)			54
$(C_5H_5)_3UCH_3$						
2.511	2.445	117.95	98.31	singlet	19 277	
2.538	2.451	117.66	98.89	triplet	0	
$(C_5H_5)_3UCl$						
2.507	2.628	116.97	100.14	singlet	19 358	
2.531	2.634	116.65	100.68	triplet	0	
	(2.559)	(116.7)	(101.0)			55

[a]SF ZORA/B3LYP/TZ2P. Experimental data from X-ray diffraction are given in parentheses where available. [b]DFT calculations for the spin-triplet did not converge. A time-dependent DFT calculation using the optimized structure for the spin-singlet ground state gave the lowest SF triplet state 0.393 eV (3170 cm^{-1}) above the ground state.

(TZ2P) for ZORA calculations as provided in the ADF basis set library. This computational protocol has been employed in some of our recent studies of actinyl species,[36,37] and has produced structures that were in good agreement with experimental data and with reliable ab initio calculations from the literature.

CASSCF and CASPT2 wave function calculations were carried out with a developer's version of Molcas 7.9[50] using the protocol detailed in refs 36 and 37. The second-order Douglas−Kroll−Hess scalar relativistic Hamiltonian[51] was employed in the calculations without SO coupling. All-electron ANO-RCC Gaussian-type basis sets contracted to TZP quality were used. SO coupling was treated by state interactions between the CASSCF/PT2 wave functions, using the Restricted Active Space State Interaction (RASSI) program.[52] For brevity, "spin-free" (i.e., non-SO, meaning scalar relativistic) and SO CASSCF and CASPT2 calculations are occasionally referred to as SCF-SF, SCF-SO, PT2-SF, and PT2-SO. To reduce symmetry breaking, we employed single state PT2-SO calculations where CASSCF wave functions are used to calculate the SO Hamiltonian, but PT2-SF energies are used to correct its diagonal elements.

The active space for $(C_5Me_4H)_3UCl$, $(C_5H_5)_3UCl$, and $(C_5H_5)_3UCH_3$ was CAS(2,7) which corresponds to the two unpaired electrons of the SF spin-triplet ground states and orbitals with large uranium 5f character. For this active space, there are 21 possible spin-triplet and 28 spin-singlet configurations, and a corresponding number of states were computed at the SF level prior to the SO RASSI step. For $(C_5Me_4H)_3UNO$, the active space was CAS(4,9) which includes the five nonbonding uranium 5f orbitals along with the bonding and antibonding orbitals arising from the interaction between the uranium $5f_\pi$ orbitals and the π^* orbitals of the NO ligand. There were 21 triplet and 28 singlet states also computed for this system prior to the SO RASSI step. The g-factors were calculated according to ref 24.

A local modification[36,53] of Molcas was used to generate orthonormal natural orbitals (NOs) ϕ_p from SF and SO RASSI calculations, and corresponding volume data for visualizations. (The index p counts the molecular orbitals.) For consistency, NOs corresponding to SF wave functions were obtained with the same code from "SO-RASSI" calculations with the SO operator suppressed. Isosurface plots of NOs were created with the graphical user interface of the ADF suite. In eq 1 below, $\rho(\mathbf{r})$ is the electron density:

$$\rho(\mathbf{r}) = \sum_p n_p[\varphi_p(\mathbf{r})]^2 \quad \sum_p n_p = N = \int \rho(\mathbf{r})\, dV \tag{1}$$

The numbers n_p (NO occupations, all positive) show how much a given orbital contributes to the electron density, while the visualization of the shape of an orbital indicates how the contribution is distributed in space. N is the number of electrons given by the volume integral of the electron density. In spin-unrestricted SF Hartree−Fock or Kohn−Sham DFT calculations, the n_p are 1 (occupied orbitals) or 0. Due to a combination of static and dynamic electron correlation and SO coupling, and/or for orbitally degenerate states, minor to large deviations from these values may be obtained in the CAS calculations. For further details and discussion of related natural spin orbitals, see ref 36.

3. RESULTS AND DISCUSSION

In this section, we use the labels a_1, a_2, and e of the C_{3v} point group symmetry species to label different 5f orbitals. It is also sometimes helpful to refer to the orbital symmetry with respect to the principal axis (U-L) but use the usual σ, π, δ, ϕ notation. The f_π and f_δ orbitals of the $C_{\infty h}$ point group correspond to the e species of C_{3v}, the f_σ orbital corresponds to a_1, and the two f_ϕ orbitals are split into a_1 ($f_{x(x^2-3y^2)}$) and a_2 ($f_{y(3x^2-y^2)}$). Obviously, due to the symmetry lowering from $C_{\infty h}$ to C_{3v} there is mixing of σ, π, δ, and ϕ species, but the $C_{\infty h}$ parent symmetry species is frequently evident in the orbital isosurface plots. It is noted that SO coupling mixes σ with π, π with δ, δ with ϕ, which we analyze below for $(C_5Me_4H)_3UNO$ with the help of natural orbital occupation numbers.

3.1. Optimized Structures. Selected DFT-optimized interatomic distances are collected in Table 1 together with experimental data, where available. The full set of data can be found in Table S1 of the Supporting Information. Structures for two possible SF states were investigated, viz. spin-singlet versus spin-triplet. For the NO complex, scalar spin-quintet states were found to be much higher in energy at the DFT level,[15] and we have consequently not taken them into consideration in the present work. For this complex, spin-unrestricted DFT calculations for a triplet state did not converge. A scalar relativistic time-dependent DFT calculation (B3LYP/TZP) of the triplet excitation spectrum placed the lowest spin-triplet 0.393 eV (3170 cm^{-1}) above the ground state. The singlet state corresponds to the case where a degenerate set of the two highest occupied molecular orbitals (HOMOs) is filled. These are bonding combinations of the two U $5f_\pi$ orbitals with the π^* orbitals of NO (see discussion below). The optimized distances are in reasonable agreement with available experimental data determined by X-ray diffraction. Our all-electron ZORA hybrid

dx.doi.org/10.1021/ic502365h | Inorg. Chem. 2014, 53, 13174−13187

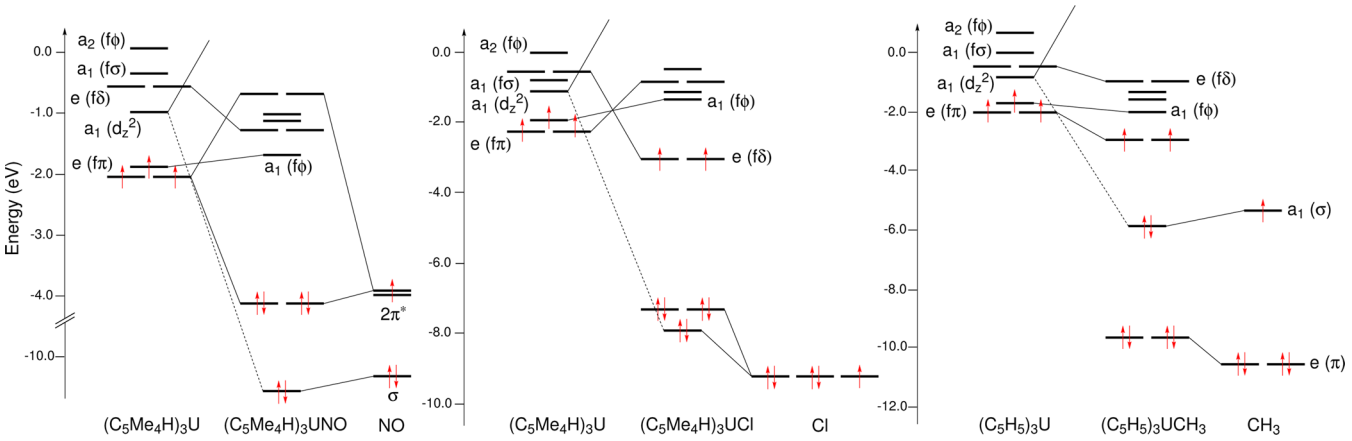

Figure 2. Molecular orbital diagrams for $(C_5Me_4H)_3UNO$, $(C_5Me_4H)_3UCl$, and $(C_5H_5)_3UCH_3$, from SF DFT calculations for the complexes and corresponding Ar_3U and L fragments [spin-averaged orbital energies for spin-paired occupations].

DFT optimized structures are also in good agreement with previous calculations performed by Evans et al.[15] using a pseudopotential for uranium and the meta-GGA TPSS or the hybrid TPSSh functionals. The computed Ar−U−Ar and Ar−U−NO angles (using the aryl centroids as reference points) fully reproduce the experimentally determined structure since the largest deviation between optimized and experimental geometries does not exceed 1°. The U−Ar distance is overestimated by 0.07 Å in the optimized structure which is close to typical differences of 0.05 Å between calculations and experiment.[56,57] At the SF level, the lowest DFT energies of $(C_5Me_4H)_3UCl$, $(C_5H_5)_3UCl$, and $(C_5H_5)_3UCH_3$ correspond to spin-triplet states. The optimized bond lengths and Cp−U−Cp and Cp−U−Cl angles associated with the triplet states are in reasonable agreement with available experimental data. The optimized U−Cl distances compare well with previous computational studies. For instance, Elkechai et al. obtained 2.615 Å for $(C_5H_5)_3UCl$.[56,57]

3.2. Ar_3U−Ligand Bonding According to the Scalar Relativistic DFT Calculations. The nature of the ground states according to the SF DFT calculations can be interpreted with orbital interaction diagrams as shown in Figure 2. The electronic structure of the complexes is described here via the interaction of the frontier fragment orbitals (FFOs) of a Ar_3U moiety (Ar = C_5H_5 or C_5Me_4H) with those of the L = NO, Cl, and CH_3 ligands. The relevant FFOs of Ar_3U were previously discussed in refs 43, 42, and 58, following the original work of ref 59. In C_{3v} symmetry, the seven U 5f orbitals of Ar_3U are split into two a_1, one a_2, and two e species. The highest occupied FFOs correspond to one of the e species, which are linear combinations of the $5f_\pi$ and $5f_\delta$ orbitals, and one a_1 orbital corresponding to a linear combination of $5f_\sigma$ with one of the $5f_\phi$ orbitals. These FFOs are predominantly nonbonding in character. The first unoccupied Ar_3U FFO is of symmetry a_1 and corresponds to a 6d-rich uranium $6d_{z^2}/6p_z$ hybrid. In older work,[42] a $5f^26d^1$ configuration was thought to be the ground state of the Ar_3U fragment, but this was later revised.[58] An unoccupied $5f_\phi$ orbital of symmetry A_2 is energetically separated from the other 5f orbitals. The destabilization is due to antibonding π-type interactions with a_2 combinations of orbitals of the aryl ligands. The corresponding occupied bonding orbital is mainly of Ar_3 character and lies below the set of occupied 5f orbitals.

The interaction between the FFOs of the Ar_3U fragment and the nitrosyl ligand in $(C_5Me_4H)_3UNO$ is indicated by two major contributions. A σ donation occurs from the doubly occupied σ frontier orbital of NO to a uranium $6d_{z^2}/6p_z$ hybrid which also has aryl contributions (Figure S1 of the Supporting Information shows the corresponding natural orbital). Further, the antibonding π^* orbitals of the nitrosyl ligand can interact with the $5f_\pi$ orbitals of the Ar_3U moiety, leading to a set of two bonding and two antibonding $5f_\pi-\pi_{NO}$ combinations with 4 electrons to fill the bonding level. The two π-bonding combinations correspond to the highest occupied molecular orbital (HOMO) set of the $(C_5Me_4H)_3UNO$ complex. The Kohn−Sham DFT orbitals as well as the SF and SO natural orbitals discussed below (Figure 6) indeed afford U−N bonding and N−O antibonding character. In the SF DFT calculation, the HOMO level is energetically well-separated from the set of lowest unoccupied MOs consisting of five nonbonding 5f orbitals and the antibonding π^*(U−NO) combinations. The strong covalent π interaction between the NO ligand and the Ar_3U fragments leads to a diamagnetic complex at the SF level.

A different electronic structure is found for $(C_5Me_4H)_3UCl$. The SF DFT ground state is a spin-triplet. Compared to the NO complex, a more pronounced σ-bonding interaction involving Cl 3p and a U $6d_{z^2}/6p_z$ hybrid is found for $(C_5Me_4H)_3UCl$ (Supporting Information Figure S1). The MO diagram in Figure 2 indicates that the valence p orbitals of chlorine are at considerably lower energy than the π^* orbitals of NO. One can therefore conceptualize the bond formation by first transferring an electron from U to Cl to form chloride, which then forms an ionic bond with some covalent character with the $5f^2$ U center. (The Supporting Information shows the corresponding MO diagram based on ionic fragments where the set of Cl^- 3p orbitals is significantly higher in energy than those of neutral Cl, and an energetic stabilization is subsequently obtained by covalent interactions with the UAr_3^+ moiety.) In a ligand-field framework, the chloride $3p_\pi$ orbitals can form bonding combinations with 5f orbitals of local π but not δ symmetry. The destabilized $5f_\pi$ level in the MO diagram represents the corresponding antibonding combination. The interaction shifts the balance of π versus δ contributions in the nonbonding 5f orbitals toward δ. This δ-dominant nonbonding U 5f pair constitutes the e-symmetry HOMO level. With an electron count of two, a spin-triplet ground state results. As

dx.doi.org/10.1021/ic502365h | Inorg. Chem. 2014, 53, 13174−13187

expected, the electronic structure of $(C_5H_5)_3UCl$ was found to be very similar to the one of $(C_5Me_4H)_3UCl$, and it is therefore not discussed further.

The orbital interaction diagram for $(C_5H_5)_3UCH_3$ is also shown in Figure 2. The occupied FFOs of the pyramidal CH_3 ligand are composed of an *e*-symmetric pair formed by linear combinations of carbon $2p_x$ and $2p_y$ orbitals with hydrogen 1s, and a singly occupied orbital of symmetry a_1 mixing carbon 2s, $2p_z$ and hydrogen 1s. The main interaction between the two fragments is the formation of a σ electron pair bond via a bonding combination of the methyl a_1 orbital with a 6d-rich U $6d_{z^2}/6p_z$ hybrid affording minor $5f_\sigma$ contributions (Supporting Information Figure S1). The result may be conceptualized via promotion at the U center from $5f_\phi$ to $6d_{z^2}$ and formation of a covalent two-electron bond with the methyl radical, or via an initial U → methyl electron transfer followed by formation of a dative electron-pair bond. Contrary to the Cl complexes, the nonbonding 5f orbitals do not interact strongly with the methyl *e* orbitals[44] (the electron density of the latter is shifted somewhat toward the plane of the hydrogens) and remain dominant in π character.

3.3. Electronic States from the ab Initio Calculations. We now turn to the low-energy part of the electronic spectrum obtained from the SF and SO CAS wave function calculations. In the following subsections, we occasionally refer to the levels of the U^{4+} ion from which the various $5f^2$ states of the complexes derive. A qualitative level splitting diagram can be found in Figure 3. According to Hund's rules, at the SF level

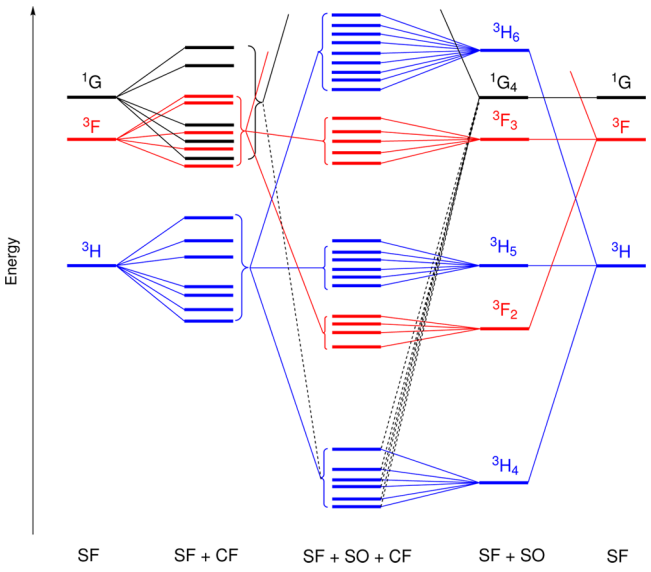

Figure 3. Energies of the spin-free (SF) and spin−orbit (SO) states of a $5f^2$ complex with the crystal-field (CF) treated a priori (left) and a posteriori (right).

the ground state of U^{4+} is the ^3H term, i.e., $L = 5$, $S = 1$ with 33 microstates when counting spin and spatial degeneracies. The trigonal CF of the complexes splits this multiplet into three spatially nondegenerate spin-triplets of symmetry A_1 and A_2, and into four 2-fold spatially degenerate spin-triplets *E*. The SO interaction couples these among each other as well as with levels deriving from the excited SF ^1G term ($L = 4$, $S = 0$) of U^{4+}. The SO ground states of the complexes have moderate to small contributions from the SF triplet ground states of the complexes. Therefore, we chose to analyze the SO electronic structures by considering SO coupling for U^{4+} first: The SF ^3H term of the spherical ion is split by the SO interaction into $^3H_4$, $^3H_5$, and $^3H_6$ levels, with the subscript indicating *J*, the total angular momentum. For a less than half filled f-shell, the ground state is the 9-fold degenerate $J = 4$ level with spin and orbital angular momentum antiparallel. The 9-fold degeneracy is then split by the CF into 3 singlets and 3 doublets. Further, the SO interaction mixes $^3H_4$ with contributions from the excited $^1G_4$ level of U^{4+} (same *J*).

3.3.1. $(C_5Me_4H)_3UCl$, $(C_5H_5)_3UCl$, and $(C_5H_5)_3UCH_3$. For $(C_5Me_4H)_3UCl$, $(C_5H_5)_3UCl$, and $(C_5H_5)_3UCH_3$, the main results obtained at the SCF-SF and SCF-SO level are collected in Table 2. Corresponding PT2 data are provided in Table S2 of the Supporting Information. The PT2 calculations did not lead to better agreement with experimental data than the SCF calculations and afforded artifacts from symmetry breaking despite our best efforts. The PT2 data are therefore not discussed in detail. For $(C_5Me_4H)_3UCl$, results both for the optimized geometry and for the experimental X-ray crystal structure are provided in order to demonstrate the impact of small structural changes on the spectrum and its assignment. SCF-SF and SCF-SO state level diagrams based on the data calculated with the optimized structures are displayed in Figure 4.

In agreement with the DFT calculations, the SF ground states of $(C_5Me_4H)_3UCl$ and $(C_5H_5)_3UCl$ are $^3A_1$ spin-triplets. The first excited states are of symmetry ^3E and are separated from the ground state by small energy gaps of 133 and 179 cm^{-1}, respectively (see Table 2). For the experimental structure of $(C_5Me_4H)_3UCl$, a larger energy gap of 288 cm^{-1} was computed. The two next higher levels, $^3A_1$ and ^3E, have similar energies. The ordering for $(C_5Me_4H)_3UCl$ depends on which geometry is used. Compared to the L = Cl systems, $(C_5H_5)_3UCH_3$ exhibits an opposite ordering of the spatial symmetry of the ground and first excited state, with $^3A_1$ at 74 cm^{-1} above a ^3E ground state. In all cases, 11 spin-triplets are obtained within 3000 cm^{-1} of the ground state energy (see Table 2 and Figure 4). These states have their origin in the SF ^3H term of a spherical U^{4+} ion, with the degeneracy of the $L = 5$ manifold broken by the trigonal C_{3v} crystal field. States deriving from other U^{4+} SF terms, namely, ^3F, ^3P, ^1G, ^1D, ^1I, and ^1S, were calculated to have much higher energy and are therefore not shown. For example, SF states of ^3F parentage are computed in the range 5000−7500 cm^{-1} above the ground state, and states arising from the lowest spin-singlet U^{4+} term ^1G are found between 5000 and 9000 cm^{-1} above the ground state.

Isosurface plots of selected natural orbitals (NOs) of the SF ground state of $(C_5H_5)_3UCl$ and $(C_5H_5)_3UCH_3$ are shown in Figure 5. In both cases, a seventh orbital with dominant 5f character has no occupation. The program generating the NOs creates linear combinations of this with other orbitals of occupation $n_p = 0$, and therefore, it is not visualized. In $(C_5H_5)_3UCl$, the unpaired electrons are described predominantly ($n_p = 0.90$) by two 5f orbitals that belong to the *e* symmetry species. For a Hartree−Fock single-determinant spin-triplet wave function or in a Kohn−Sham DFT calculation, the occupations of these orbitals would be 1 exactly. Due to electron correlation entering the multideterminant CAS wave function, the occupations are lowered to 0.9, but the electronic structure remains described predominantly by a single orbital diagram as in Figure 2. In the C_{3v} point group, orbitals with δ

dx.doi.org/10.1021/ic502365h | Inorg. Chem. 2014, 53, 13174−13187

Table 2. Relative Energies (cm^{-1}) and Assignment of Low-Energy SF and SO States, CAS(2,7)SCF Calculations

SCF-SF			SCF-SO					
state	ΔE	major configurations[a,b]	state	ΔE	weight of $^{2S+1}L_J$	$g_{\|\|}$[c]	eingenvectors in the $J = 4$, $\|M_J\rangle$ basis[d]	$g_{\|\|}$[e]
$(C_5Me_4H)_3UCl$[f]								
$^3A_1$	0	61($f^1_\delta f^1_\delta$), 19($f^1_\pi f^1_\pi$)	$^1A_1$	0	91.6 $^3H_4$, 7.7 $^1G_4$		0.975|0⟩ + 0.157|3⟩ − 0.157|−3⟩	
^3E	288	64($f^1_\delta f^1_\phi$), 10($f^1_\sigma f^1_\pi$)	^2E	218	91.1 $^3H_4$, 7.6 $^1G_4$	1.123	0.918|±1⟩ + 0.356|∓2⟩ + 0.174|±4⟩	1.136
^3E	676	38($f^1_\delta f^1_\pi$), 31($f^1_\delta f^1_\sigma$), 23($f^1_\pi f^1_\phi$)	^2E	628	90.4 $^3H_4$, 7.7 $^1G_4$	0.350	0.780 |∓2⟩ + 0.485|±4⟩ + 0.395|±1⟩	0.192
$^3A_1$	741	63($f^1_\phi f^1_\sigma$), 30($f^1_\delta f^1_\pi$)	$^1A_2$	779	91.2 $^3H_4$, 5.3 $^1G_4$		0.707|3⟩ + 0.707|−3⟩	
^3E	2095	30($f^1_\sigma f^1_\pi$), 23($f^1_\delta f^1_\phi$), 16($f^1_\pi f^1_\phi$)	^2E	1268	86.3 $^3H_4$, 11.3 $^1G_4$	3.456	0.857|±4⟩ − 0.514 |∓2⟩ + 0.036|±1⟩	3.855
^3E	2557	44($f^1_\delta f^1_\sigma$), 38($f^1_\pi f^1_\phi$)	$^1A_1$	1740	83.5 $^3H_4$, 12.8 $^1G_4$		−0.689|3⟩ + 0.689|−3⟩ + 0.222|0⟩	
$^3A_2$	3069	47($f^1_\pi f^1_\pi$), 30($f^1_\delta f^1_\pi$), 15($f^1_\sigma f^1_\phi$)						
$(C_5Me_4H)_3UCl$[g]								
$^3A_1$	0	63($f^1_\delta f^1_\delta$), 18($f^1_\pi f^1_\pi$)	$^1A_1$	0	91.2 $^3H_4$, 8.0 $^1G_4$		0.966|0⟩ + 0.181|3⟩ − 0.181|−3⟩	
^3E	133	69($f^1_\delta f^1_\phi$), 11($f^1_\sigma f^1_\pi$)	^2E	168	91.1 $^3H_4$, 7.5 $^1G_4$	1.040	0.871|±1⟩ + 0.422|∓2⟩ + 0.248|±4⟩	1.039
$^3A_1$	532	60($f^1_\phi f^1_\sigma$), 25($f^1_\delta f^1_\pi$)	^2E	483	90.1 $^3H_4$, 8.1 $^1G_4$	0.773	0.668|∓2⟩ + 0.564|±4⟩ + 0.485|±1⟩	0.984
^3E	552	36($f^1_\delta f^1_\pi$), 27($f^1_\delta f^1_\sigma$)	$^1A_2$	602	91.1 $^3H_4$, 5.9 $^1G_4$		0.707|3⟩ + 0.707|−3⟩	
^3E	1697	29($f^1_\delta f^1_\phi$), 24($f^1_\sigma f^1_\pi$), 16($f^1_\pi f^1_\phi$)	^2E	954	87.4 $^3H_4$, 10.9 $^1G_4$	2.559	0.787|±4⟩ − 0.612|∓2⟩ + 0.072|±1⟩	2.775
^3E	2241	41($f^1_\pi f^1_\phi$), 38($f^1_\delta f^1_\sigma$)	$^1A_1$	1450	85.0 $^3H_4$, 12.5 $^1G_4$		−0.683|3⟩ + 0.683 |−3⟩ + 0.256|0⟩	
$^3A_2$	2747	46($f^1_\pi f^1_\pi$), 22($f^1_\delta f^1_\pi$), 18($f^1_\sigma f^1_\phi$)						
$(C_5H_5)_3UCl$								
$^3A_1$	0	79($f^1_\delta f^1_\delta$), 10($f^1_\pi f^1_\pi$)	$^1A_1$	0	91.2 $^3H_4$, 7.9 $^1G_4$		0.957|0⟩ + 0.205|3⟩ − 0.205|−3⟩	
^3E	179	81($f^1_\delta f^1_\phi$)	^2E	186	91.2 $^3H_4$, 6.2 $^1G_4$	0.854	0.837|±1⟩ + 0.476 |∓2⟩ + 0.267|±4⟩	0.854
$^3A_1$	685	69($f^1_\phi f^1_\sigma$), 16($f^1_\delta f^1_\pi$)	^2E	523	89.9 $^3H_4$, 8.3 $^1G_4$	1.206	0.599|±4⟩ + 0.599 |∓2⟩ − 0.531|±1⟩	1.598
^3E	758	16($f^1_\phi f^1_\pi$), 17($f^1_\delta f^1_\sigma$), 16($f^1_\delta f^1_\pi$)	$^1A_2$	668	91.5 $^3H_4$, 5.5 $^1G_4$		0.707|3⟩ + 0.707|−3⟩	
^3E	2078	53($f^1_\phi f^1_\pi$), 29($f^1_\delta f^1_\phi$)	^2E	1028	87.3 $^3H_4$, 10.6 $^1G_4$	2.188	0.755|±4⟩ − 0.643 |∓2⟩ + 0.125|±1⟩	2.347
^3E	2641	37($f^1_\sigma f^1_\pi$), 25($f^1_\phi f^1_\delta$), 17($f^1_\pi f^1_\phi$)	$^1A_1$	1686	83.6 $^3H_4$, 13.6 $^1G_4$		−0.676|3⟩ + 0.676|−3⟩ + 0.290|0⟩	
$^3A_2$	3431	61($f^1_\pi f^1_\pi$), 24($f^1_\sigma f^1_\phi$)						
$(C_5H_5)_3UCH_3$								
^3E	0	80($f^1_\phi f^1_\delta$)	$^1A_1$	0	91.5 $^3H_4$, 7.5 $^1G_4$		0.942|0⟩ + 0.235|3⟩ − 0.235|−3⟩	
$^3A_1$	74	79($f^1_\delta f^1_\delta$), 11($f^1_\pi f^1_\pi$)	^2E	192	91.6 $^3H_4$, 5.9 $^1G_4$	2.194	0.643|±4⟩ + 0.556|±1⟩ + 0.525|∓2⟩	2.257
$^3A_1$	801	67($f^1_\phi f^1_\sigma$), 16($f^1_\delta f^1_\pi$)	^2E	347	88.9 $^3H_4$, 10.0 $^1G_4$	3.016	0.782|±1⟩ + 0.619|±4⟩ + 0.071|∓2⟩	3.414
^3E	880	25($f^1_\phi f^1_\pi$), 20($f^1_\delta f^1_\sigma$), 16($f^1_\delta f^1_\pi$)	$^1A_2$	490	91.4 $^3H_4$, 5.4 $^1G_4$		0.707|3⟩ + 0.707|−3⟩	
^3E	1780	37($f^1_\phi f^1_\pi$), 32($f^1_\delta f^1_\phi$)	^2E	925	88.1 $^3H_4$, 10.8 $^1G_4$	0.849	0.847|∓2⟩ + 0.541|±4⟩ + 0.279|±1⟩	0.872
^3E	2789	30($f^1_\sigma f^1_\pi$), 22($f^1_\pi f^1_\phi$), 21($f^1_\phi f^1_\delta$)	$^1A_1$	1418	85.3 $^3H_4$, 12.5 $^1G_4$		−0.666|3⟩ + 0.666|−3⟩ + 0.333|0⟩	
$^3A_2$	3330	61($f^1_\pi f^1_\pi$), 24($f^1_\sigma f^1_\phi$)						

[a]Numbers indicate the weight of the configurations in %, only contributions larger than 10% are listed. [b]In the C_{3v} symmetry, the $5f_\sigma$ orbital is labeled $5f_{a1}$, $5f_\pi$, and $5f_\delta$ are labeled $5f_e$, and the two $5f_\phi$ orbitals are split into $5f_{a1}$ and $5f_{a2}$. [c]Electronic g-factor obtained as described in ref 24 with $g_\perp = 0.000$. [d]Eigenvectors obtained from the crystal field procedure detailed in the text and the data from Table 3. [e]Electronic g-factor obtained by using eq 4 and wave functions in the $J = 4$, $|M_J\rangle$ basis set, with $g_\perp = 0.000$. [f]Experimental geometry. [g]Optimized geometry.

and π parentage both belong to the e species. The NOs in Figure 5 representing the unpaired electrons support π interactions with the Cl ligand but exhibit a large degree of δ. The electronic configuration derives from the component $M_L = 0$ of the term ^3H of U^{4+}, here with a mixture of $M_L = \sum m_l = \pm 2 \mp 2$ and $M_L = \sum m_l = \pm 1 \mp 1$, involving 5f δ and π orbitals with mutual cancellation of their orbital angular momenta. Indeed, as detailed in Table 2, the SF ground state wave function of $(C_5H_5)_3UCl$ corresponds to an admixture of the $5f^1_\delta 5f^1_\delta$ and $5f^1_\pi 5f^1_\pi$ configurations with a combined weight of 89%.

In $(C_5H_5)_3UCH_3$ the unpaired electrons are described by 5f orbitals of symmetry a_1 and e, with occupation numbers of 0.9 each. The ground state derives from the $M_L = \pm 5$ component of the ^3H term, with $M_L = \sum m_l = \pm 3 \pm 2$. The approximate ϕ and δ character is evident in the NOs displayed in Figure 5. In the SF DFT calculation the two unpaired orbitals have e symmetry; i.e., the electron density corresponds to the SCF-SF $^3A_1$ excited state. However, the splitting of the nonbonding 5f orbitals in $(C_5H_5)_3UCH_3$ is small, and the $^3A_1$ and ^3E states are very close in energy. Therefore, a DFT calculation may easily converge to a density reflecting some state other than the desired one. Such behavior was already noted previously in studies of actinyl ions.[37,60,61]

The spin−orbit states were calculated by diagonalizing the SO operator in the basis of all calculated SF states. The SO ground state of the optimized $(C_5Me_4H)_3UCl$, $(C_5H_5)_3UCl$, and $(C_5H_5)_3UCH_3$ complexes is nondegenerate, of symmetry A_1 in the C_{3v} double group. It is separated from a doublet E by 168, 186, and 192 cm^{-1}, respectively. In each case, the SCF-SO state ordering starting from the ground state is A_1, E, E, A_2, E, and A_1 (see Table 2). These states derive from a CF splitting of the U^{4+} term $^3H_4$. The 9-fold degeneracy of this term is expected to split by a trigonal crystal field into three doublets of symmetry E and into three singlets, $2A_1 + A_2$. The spin−orbit coupling mixes states with the same $J = 4$, and therefore, these nine states contain a relatively important admixture from states deriving from the singlet $^1G_4$ term. Furthermore, the CF interaction strongly mixes the nine components of the $^3H_4$ ground multiplet, leading to an SO ground state which contains a relatively small contribution from the SF ground state. The

dx.doi.org/10.1021/ic502365h | Inorg. Chem. 2014, 53, 13174−13187

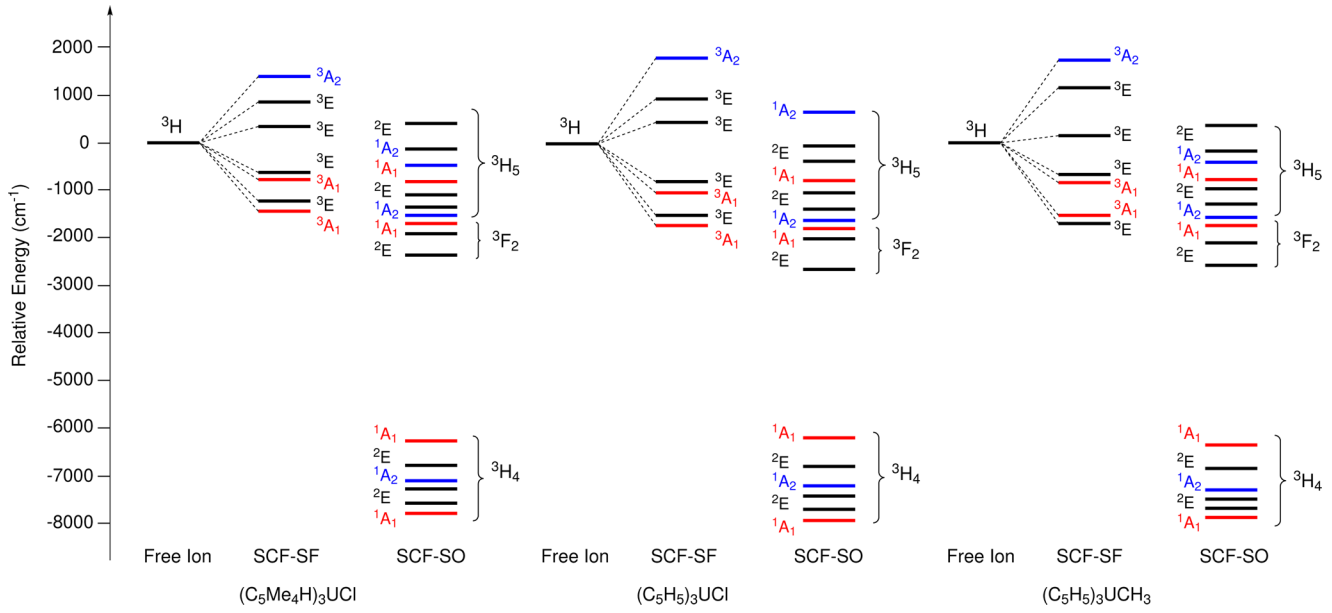

Figure 4. Energies and assignment of low-energy electronic states. CAS(2,7)SCF calculations. $E = 0$ corresponds a hypothetical term ^3H of U^{4+} in the complex and corresponds to the center of the SF states.

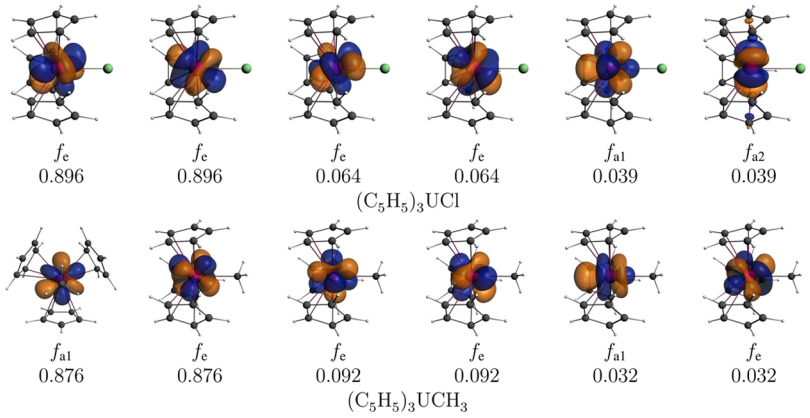

Figure 5. Selected NOs ϕ_p and occupation numbers n_p of eq 1 for $(C_5H_5)_3UCl$ (top) and $(C_5H_5)_3UCH_3$ (bottom). As indicated in Figure 4, the SF ground state of $(C_5H_5)_3UCl$ is of symmetry $^3A_1$ ($M_L = 0$ and $M_S = 1$), whereas the SF ground state of $(C_5H_5)_3UCH_3$ is of symmetry ^3E ($M_L = \pm 5$ and $M_S = 1$). Isosurface values: ± 0.03 au. The NO isosurfaces for $(C_5Me_4H)_3UCl$ are very similar to those of $(C_5H_5)_3UCl$ and therefore not shown. Side view with the horizontal view plane coinciding with one of the σ_v symmetry planes, except for f_{a1} [$n_p = 0.876$ of $(C_5H_5)_3UCH_3$] which is viewed approximately along the U−Me direction to show the 3-fold symmetry.

most dramatic case is $(C_5H_5)_3UCH_3$ where the SF ground state ^3E contributes only 12% to the SO ground state A_1. For $(C_5Me_4H)_3UCl$ and $(C_5H_5)_3UCl$ the SO ground state contains a 40% contribution of the SF ground state $^3A_1$. The influence of the CF and SO interactions is clearly reflected in the natural orbitals given in Figures S3−S5 of the Supporting Information. For example, for $(C_5H_5)_3UCl$ there is a strong increase of the occupations of the second pair of $5f_e$ and of the $5f_{a1}$ orbitals.

For the A_1 ground state of $(C_5Me_4H)_3UCl$, $(C_5H_5)_3UCl$, and $(C_5H_5)_3UCH_3$, the balance between the $^3H_4$ and $^1G_4$ contribution is approximately 90% versus 8%, respectively, and it increases to 85% versus 13% for the second A_1 state. For $(C_5Me_4H)_3UCl$, the state ordering does not change among the experimental and optimized structures. However, the magnitude of the splitting of the $^3H_4$ term differs between the two geometries. Compared to the X-ray structure, the SO excited states of the optimized structure shift to lower energy. The low-energy part of the absorption spectrum of $(C_5H_5)_3UCl$ has been observed experimentally by Amberger et al.[41] The first excited states have been assigned to two doublets E at 210 and 450 cm^{-1}. A third excited state was observed at 4425 cm^{-1} above the ground state and was assigned to the first doublet of symmetry E deriving from the $^3F_2$ multiplet. The calculations are in reasonable agreement with experiment: we find the first two excited doublet states at 186 and 523 cm^{-1}, respectively, whereas the first doublet deriving from the $^3F_2$ multiplet is found at 5246 cm^{-1}. Overall, the lowest electronic states deriving from the $^3H_4$ term are well-separated from states deriving from the $^3F_2$ term by 3965, 3561, and 3768 cm^{-1} for $(C_5Me_4H)_3UCl$, $(C_5H_5)_3UCl$, and $(C_5H_5)_3UCH_3$, respectively.

PT2 data are provided in Supporting Information Table S2 for $(C_5Me_4H)_3UCl$, $(C_5H_5)_3UCl$, and $(C_5H_5)_3UCH_3$. The perturbative inclusion of dynamical correlation does not lead to a better agreement with the experimental data for $(C_5H_5)_3UCl$. For instance, the two lowest doublets E are shifted to higher energy. The second doublet is around 800 cm^{-1} above the

dx.doi.org/10.1021/ic502365h | Inorg. Chem. 2014, 53, 13174−13187

ground state, which strongly overestimates the experimental value of 450 cm^{-1}. Furthermore, there is considerable symmetry breaking as indicated by energetic splitting of doublet states. A failure of PT2 to reproduce properly the lower part of the energetic spectrum of f-element complexes has already been noted previously.[62,63] It is furthermore known that the magnetic susceptibility is relatively insensitive to correlation,[64−67] and therefore, CASSCF calculations as used in this work should describe the magnetic properties reasonably well.

3.3.2. Crystal-Field Models Derived from the CAS Calculations, and Calculated g-Factors. The splitting of the $^3H_4$ term, and the resulting magnetic properties of the complexes, can be rationalized with the help of crystal field theory and simple model wave functions. In lowest order of approximations, the wave functions associated with the SO−CF states are made up of linear combinations from $J = 4$ wave functions with $M_J = \pm4, \pm3, \pm2, \pm1$, and 0. The crystal field operator can be expressed as

$$\hat{H}^{CF} = \sum_{k=2,4,6} \beta_k \sum_{q=-k}^{k} B_k^q \hat{O}_k^q \tag{2}$$

where the $\hat{O}_k^q$ are the Stevens operators, B_k^q are the CF parameters, and β_k parameters are obtained from the Wigner−Eckart theorem, depending on the f^n configuration.[68] In C_{3v} symmetry, the nonvanishing B_k^q terms have $k = 2, 4, 6$ and $q = 0, \pm3, \pm6$. A restriction to the $^3H_4$ multiplet has the advantage that we can use matrix elements $\langle JM_J|\hat{O}_k^q|JM_J'\rangle$ tabulated for the C_{3v} point group by Stevens[68] and Judd,[69] and by Abragam and Bleaney[70] for other symmetries. We have determined the crystal field parameters from the energy spectra of the CAS calculations by a least-squares procedure (see Supporting Information). The CF parameters B_k^q determined in this way are collected in Table 3. The corresponding eigenvectors of the CF states in the $|M_J\rangle$ basis for $J = 4$ are given in Table 2.

The nature and the ordering of the singlet states are similar for the Ar_3U−L complexes with L = Cl and CH_3. The ground state A_1 has a dominant contribution from $M_J = 0$, the excited A_2 state is a pure linear combination of $M_J = \pm3$, and the A_1 excited state has a dominant $M_J = \pm3$ character. The three doublets of symmetry E are characterized by eigenvectors $|\psi_\pm\rangle$ of the type[71]

$$|\psi_\pm\rangle = a|4, \pm4\rangle + b|4, \mp2\rangle + c|4, \pm1\rangle \tag{3}$$

where $a^2 + b^2 + c^2 = 1$ for normalization. Contrary to the nondegenerate states, the ordering of the doublets differs among $(C_5H_5)_3UCH_3$ and the chloride complexes. For $(C_5Me_4H)_3UCl$ and $(C_5H_5)_3UCl$, the first doublet is characterized by a large $M_J = \pm1$ contribution, with c^2 ranging from 84% to 70%, and by two smaller $M_J = \mp2$ and $M_J = \pm4$ contributions. The second doublet has a strong $M_J = \mp2$ character for the experimental structure of $(C_5Me_4H)_3UCl$. In $(C_5H_5)_3UCl$, this contribution decreases to 36% in favor of an increase of the $M_J = \pm4$ (36%) and $M_J = \pm1$ (28%) components. The third doublet E is dominated by $M_J = \pm4$, with contribution ranging from 73% for the experimental geometry of $(C_5Me_4H)_3UCl$ to 57% for $(C_5H_5)_3UCl$. These results are in good agreement with previous assignments by Amberger et al.[41] who attributed a dominant $M_J = \pm1$ and $M_J = \mp2$ character to the first and second doublet, respectively.

A different doublet ordering is found for $(C_5H_5)_3UCH_3$, where the major components change with increasing energy from $M_J = \pm4$ (41%) to $M_J = \pm1$ (61%) to $M_J = \mp2$ (72%). This difference in the ordering of the doublets arises from the different magnitude of the CF parameter B_2^0 which is much smaller for $(C_5H_5)_3UCH_3$. As seen in eq S7 of the Supporting Information, the diagonal matrix elements $\langle 4, M_J|\hat{O}_2^0|4, M_J\rangle$ for $M_J = \pm4, \pm2$, and ±1 are equal to $28b_2^0$, $-8b_2^0$, and $-17b_2^0$, respectively. Consequently, a decrease of the CF parameter B_2^0 leads to less destabilization of the $M_J = \pm4$ components.

The electronic g-factors associated with the doublet states can be evaluated as follows:[71,72]

$$g_\parallel = 2g_J(4a^2 - 2b^2 + c^2) \text{ and } g_\perp = 0 \tag{4}$$

Here, g_J is the Landé factor and equal to $^4/_5$ for a $^3H_4$ term. The values of a, b, and c are collected in Table 2, and the resulting g-factors obtained with eq 5 are given in the same table. The magnitude of $g_\parallel$ depends directly on the magnitude of the M_J contributions. A larger $M_J = \pm4$ component in the wave function will lead to a larger magnitude of $g_\parallel$. For instance, for the experimental structure of $(C_5Me_4H)_3UCl$, the parallel component for the three doublets E are $g_\parallel = 1.136$, 0.192, and 3.855, respectively. The magnitudes of $g_\parallel$ are the results of the dominant $M_J = \pm1$ and $M_J = \pm4$ character for the first and third doublets, respectively. The small magnitude of $g_\parallel$ for the second doublet corresponds to a cancellation of the $M_J = \pm4$ and $M_J = \mp2$ angular momenta in the wave function.

The magnitude of these g-factors can be compared to ab initio g-factors, obtained as $g_\parallel = 2\langle\Psi|\hat{L}_\parallel + g_e\hat{S}_\parallel|\Psi\rangle$ if $|\Psi\rangle$ is the pseudo-spin-up component of the doublet. As seen in Table 2, overall the g-factors obtained with the simple CF model agree quite well with the CAS results. The differences highlight the approximation of taking into account only the $^3H_4$ ground multiplet and not also $^1G_4$. It was mentioned in the literature that the treatment of the CF interaction as a perturbation of the SO ground multiplet might not always be a good approximation for actinide complexes.[6]

3.3.3. Electronic States of $(C_5Me_4H)_3UNO$. The energies and the assignment of the ground and first excited states obtained at the SCF-SF level for the experimental X-ray and optimized

Table 3. Relative Energies (cm^{-1}) and Crystal Field Parameters (cm^{-1}) Obtained by a Least-Squares Fit to the SCF-SO Energies for $(C_5Me_4H)_3UCl$, $(C_5H_5)_3UCl$, and $(C_5H_5)_3UCH_3$[a]

	$(C_5Me_4H)_3UCl$[b]	$(C_5Me_4H)_3UCl$[c]	$(C_5H_5)_3UCl$	$(C_5H_5)_3UCH_3$
$^1A_1$	0	0	0	0
^2E	205	156	158	186
^2E	623	480	521	349
$^1A_2$	796	617	697	495
^2E	1287	973	1059	942
$^1A_1$	1724	1430	1651	1396
B_2^0	−955	−634	−647	−140
B_4^0	344	306	352	365
B_6^0	−6	−11	−28	22
B_4^3	−355	−334	−411	−350
B_6^3	−150	−143	−202	−222
B_6^6	−360	−308	−349	−319
rms[d]	14.3	14.7	26.4	12.0

[a]See Supporting Information for details. [b]Experimental geometry. [c]Optimized geometry. [d]Root mean square deviations of the fitted energies vs SCF-SO energies (cm^{-1}).

dx.doi.org/10.1021/ic502365h | Inorg. Chem. 2014, 53, 13174−13187

structures of $(C_5Me_4H)_3UNO$ are collected in Table 4. The energies of the electronic states obtained at the SCF-SO level are provided in Supporting Information Table S3, and the corresponding PT2 results are provided in Table S4 of the Supporting Information. As suggested by Bursten et al. in a previous computational study using SF DFT with the Xα functional,[42] the SF ground state of $(C_5Me_4H)_3UNO$ corresponds to a nonmagnetic nondegenerate state ^1A that is well-separated in energy from the lowest excited states. The natural orbital occupations for the ground state of $(C_5Me_4H)_3$-UNO are given in Figure 6. In qualitative agreement with the SF DFT results of section 3.1, for the SF ground state large NO occupation numbers, i.e., n_p = 1.64, are found for the two π-type orbitals which correspond to the bonding interaction between the $5f_\pi$ orbitals of the $U(C_5Me_4H)_3$ moiety with the π^* orbitals of the nitrosyl ligand. However, the occupations are significantly below 2 while large occupations (n_p = 0.32) are obtained for the two related antibonding π^* combination. Such a situation was previously also noted by Wang et al. for the NUNH complex[73] and in refs 74 and 75 in the case of multiple metal−metal bonds.

Table 4. Relative Energies (cm^{-1}) and Percentages of Different Configurations (Indicated by ↑ and ↓ for Occupations of the α- and β-Spin Frontier Orbitals) Contributing to the Lowest SF Electronic States of $(C_5Me_4H)_3UNO$ Complex

state	ΔE	configurations[c]
$(C_5Me_4H)_3UNO$[a]		
^1A	0	$23\pi_2^\uparrow\pi_1^{*\downarrow}\pi_2^{*\downarrow}$, $14\pi_1^{\uparrow\downarrow}\pi_2^{\uparrow\downarrow}$, $15\pi_1^{\uparrow\downarrow}\pi_2^\uparrow\pi_1^{*\downarrow}$ $8\pi_1^{\uparrow\downarrow}\pi_2^\uparrow\pi_2^{*\downarrow}$, $8\pi_1^\uparrow\pi_2^{\uparrow\downarrow}\pi_1^{*\downarrow}$, $15\pi_1^\uparrow\pi_2^{\uparrow\downarrow}\pi_2^{*\downarrow}$
^3E	3746	$34\pi_1^\uparrow\pi_2^{\uparrow\downarrow}f_\phi^\downarrow$, $10\pi_1^\uparrow\pi_2^\uparrow f_\phi^\downarrow f_\delta^\downarrow$
$(C_5Me_4H)_3UNO$[b]		
^1A	0	$20\pi_1^\uparrow\pi_2^\uparrow\pi_1^{*\downarrow}\pi_2^{*\downarrow}$, $18\pi_1^{\uparrow\downarrow}\pi_2^{\uparrow\downarrow}$, $12\pi_1^{\uparrow\downarrow}\pi_2^\uparrow\pi_1^{*\downarrow}$ $13\pi_1^{\uparrow\downarrow}\pi_2^\uparrow\pi_2^{*\downarrow}$, $12\pi_1^\uparrow\pi_2^{\uparrow\downarrow}\pi_1^{*\downarrow}$, $13\pi_1^\uparrow\pi_2^{\uparrow\downarrow}\pi_2^{*\downarrow}$
^3E	4433	$42\pi_1^\uparrow\pi_2^{\uparrow\downarrow}f_\phi^\downarrow$, $13\pi_1^\uparrow\pi_2^\uparrow f_\phi^\downarrow f_\delta^\downarrow$

[a]Experimental geometry. [b]Optimized geometry. [c]According to Molcas output.

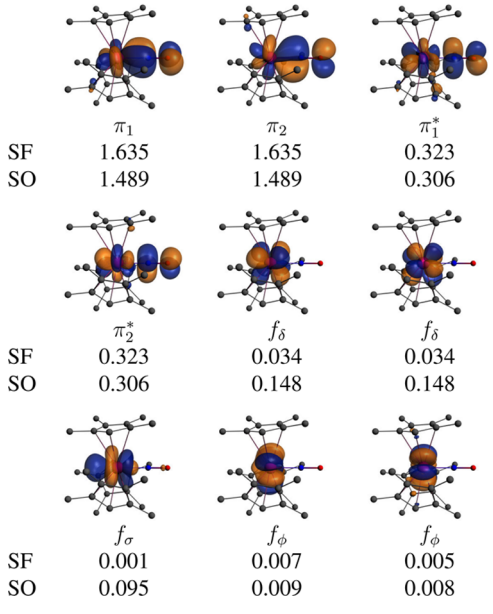

Figure 6. Ground state of $(C_5Me_4H)_3UNO$: Selected NOs ϕ_p and occupation numbers n_p of eq 1 for $(C_5Me_4H)_3UNO$. Occupation numbers listed for the SCF-SF and SCF-SO ground states of the optimized geometry. The figure shows the NOs from the SO calculation; the orbitals for the SF state appear very similar and can be found in Figure S6 of the Supporting Information. Isosurface values: ±0.03 au. Hydrogen atoms have been removed to reduce clutter.

In spin-restricted MO theory, a two-electron bond is described by a doubly occupied bonding orbital. However, this is a picture of bonding where a single-determinant wave function (Hartree−Fock, or the wave function for non-interacting quasielectrons in Kohn−Sham DFT) represents a single MO diagram and vice versa. A correlated multi-determinant wave function may reflect large contributions from various different MO diagrams if the state in question is of multiconfigurational character. A suitable description of bonding in such a situation may then be obtained with the pair of bonding and antibonding orbitals which are both fractionally occupied.[76,77] The singlet ground state of $(C_5Me_4H)_3UNO$ clearly exhibits such a multiconfigurational character with several competing configurations. The "DFT configuration" $\pi_1^{\uparrow\downarrow}\pi_2^{\uparrow\downarrow}\pi_1^{*0}\pi_2^{*0}$ (note that the Kohn−Sham DFT orbitals are only qualitatively the same as in Figure 6) contributes only 18% to the wave function for the optimized structure (see Table 4). The major configuration (20%) corresponds to a double excitation to the π^* orbitals ($\pi_1^\uparrow\pi_2^\uparrow\pi_1^{*\downarrow}\pi_1^{*\downarrow}$). Furthermore, the wave function contains configurations corresponding to single excitation from one of the bonding π orbitals to the antibonding ones. From the NO occupation numbers n_p, an effective bond order can be obtained as the difference of the total occupancies of the bonding and antibonding orbitals divided by 2.[76] According to this criterion the U−NO π-bond order is 1.31 instead of 2.

The first excited state of $(C_5Me_4H)_3UNO$ corresponds to a spin-triplet state of symmetry ^3E, calculated at 3746 and 4433 cm^{-1} above the ground state for the experimental and optimized structure, respectively. The corresponding natural orbitals for one of the spatial components of this triplet state are given in Figure 7. This state corresponds mainly to a one-electron spin-flip excitation from the bonding π orbitals to the $5f_\phi$ orbital. Indeed, compared to the singlet SF ground state, the combined electronic occupation for one of the π/π^* pairs is decreased by 0.83 in the triplet state, while the occupation of one of the $5f_\phi$ orbitals increases from 0.01 to 0.85. The excitation is qualitatively in agreement with what would be expected from the DFT orbital diagram in Figure 2. A sizable occupation number, i.e., 0.14, is also calculated for one of the $5f_\delta$ orbitals. As seen in Table 4, the wave function of the first excited spin-triplet contains a significant percentage (10−13% depending on the geometry used) of the electronic configuration $\pi_1^\uparrow\pi_2^\uparrow f_\phi^\uparrow f_\delta^\downarrow$. The energies of higher SF excited states are given in Table S3 of the Supporting Information. Above the first excited doublet ^3E, a relatively large number of excited states is calculated in the range 4000−6000 cm^{-1}. Due to their strong multiconfigurational character, the nature of these excited states is not discussed further.

The SO ground state of $(C_5Me_4H)_3UNO$ is of symmetry A and derives principally from the SF ground state (64% and 67% for the experimental and optimized structure, respectively). The SO ground state contains a large admixture predominantly from the first two spin-triplet states (combined 35% and 32%). The effect of spin−orbit coupling in the SO ground state is clearly visible in the NO occupation numbers which are also

dx.doi.org/10.1021/ic502365h | Inorg. Chem. 2014, 53, 13174−13187

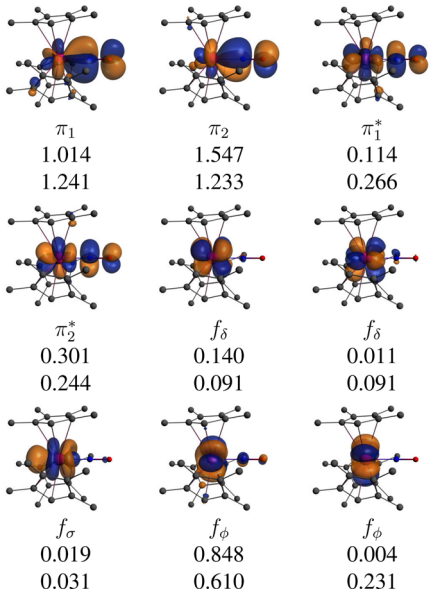

Figure 7. First excited state of $(C_5Me_4H)_3UNO$: Selected NOs ϕ_p and occupation numbers n_p of eq 1 for $(C_5Me_4H)_3UNO$. Occupation numbers listed for the SCF-SF and SCF-SO first excited states of the optimized geometry. The figure shows the NOs from the SO calculation; the orbitals for the SF state appear very similar and can be found in Figure S7 of the Supporting Information. Isosurface values: ±0.03 au. Hydrogen atoms have been removed to reduce clutter.

given in Figure 6. In linear symmetry, SO coupling mixes π with σ and δ with π. Correspondingly, there is an obvious buildup of occupations of the $5f_\delta$ and to a lesser degree for $5f_\sigma$ at the expense of the U−NO π antibonding and in particular of the U−NO π-bonding orbitals. One consequence of SO coupling is therefore a reduction of the bond order to 1.18. The first excited SO state corresponds to a magnetic doublet E and is calculated at 3415 and 3899 cm^{-1} above the SO ground state for the experimental and optimized structure, respectively (Supporting Information Table S3). The NO occupations shown in Figure 7 are not very similar to those of the first SF excited state, because this SF state contributes only 35% to the SO wave function. However, we note overall a significant increase of population of the $5f_\phi$ orbitals and a decrease for $5f_\pi$ compared to the SO ground state, which has some resemblance to the SF case.

3.4. Magnetic Susceptibility from the ab Initio Calculations. The paramagnetic susceptibility χ_u for the magnetic field in direction u coinciding with one of the magnetic axes of a complex can be computed according to the van Vleck equation

$$\chi_u = \frac{1}{Q_0}\mu_0\mu_B^2 \sum_\lambda e^{-\beta E_\lambda}\left[\beta \sum_{a,a'} \left|\langle\psi_{\lambda a}|\hat{L}_u + g_e\hat{S}_u|\psi_{\lambda a'}\rangle\right|^2 + 2\sum_{\lambda'\neq\lambda}\sum_{a,a'} \frac{\left|\langle\psi_{\lambda a}|\hat{L}_u + g_e\hat{S}_u|\psi_{\lambda' a'}\rangle\right|^2}{E_{\lambda'} - E_\lambda}\right] \quad (5)$$

The summation goes over the set of electronic states, with $Q_0 = \sum_{\lambda,a} e^{-\beta E_\lambda}$ being the partition function and $\beta = 1/kT$. The indices a,a' count the components within degenerate states. The factors μ_0 and μ_B are the vacuum permeability and Bohr magneton, respectively. The isotropic susceptibility χ is the average of the principal components χ_u of the susceptibility tensor. There is also an implementation for the susceptibility in Molcas that employs wave functions diagonalizing the Zeeman operator within the requested set of electronic states and then Boltzmann-averages the magnetic moment expectation values.[78] Equation 5 represents a second-order perturbation theoretical equivalent of this approach. Here and in previous work on actinide species we found that within the calculated set of states the results were numerically equivalent to using eq 5. In principle, the sum over states in the van Vleck equation should include all excited states of a system, but in practice we found that for our samples the calculated susceptibility converges quickly with the number of states.

Figure 8 shows the calculated isotropic susceptibilities times temperature, χT, for $(C_5Me_4H)_3UCl$ and $(C_5Me_4H)_3UNO$ in

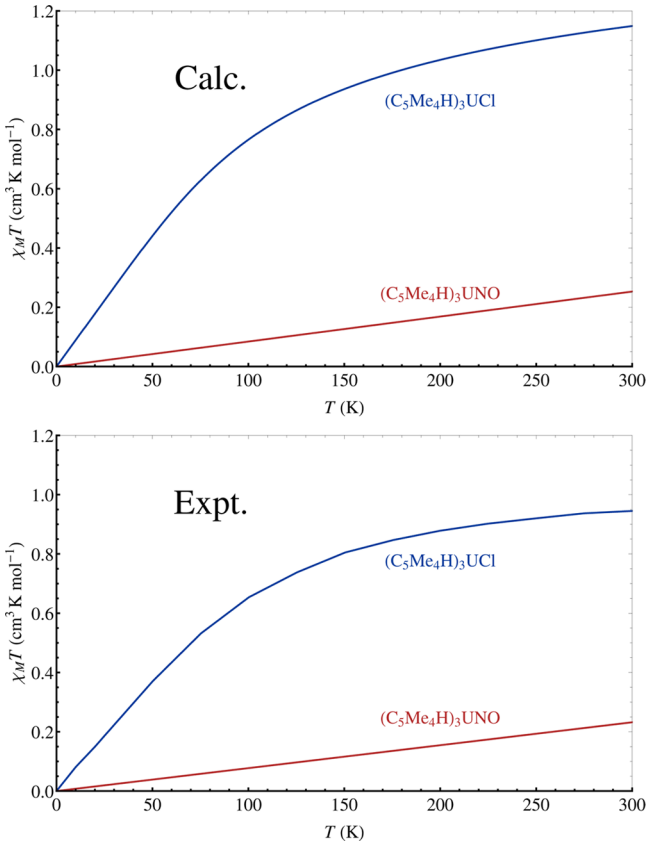

Figure 8. Comparison of the calculated and measured magnetic susceptibility χT (cm^3 K mol^{-1}) of $(C_5Me_4H)_3UCl$ and $(C_5Me_4H)_3$-UNO as a function of T (K). The experimental curves were generated using data extracted from graphical material of ref 15. Experimental structures used for the calculations.

comparison with each other, and in comparison with experiment. Clearly, the different nature of the electronic ground state and low-energy excited states is reflected in the curves, displaying TIP (linear χT) for $(C_5Me_4H)_3UCl$ only at low temperatures but for $(C_5Me_4H)_3UNO$ all the way up to room temperature in agreement with experiment. The relative magnitudes of the susceptibilities are also correctly reproduced by the calculations. Additional plots are provided in Figures 9 and 10, and numerical data are collected in Table 5. As far as the convergence of the summation in eq 5 with the number of states is concerned, the curve for $(C_5Me_4H)_3UCl$ in Figure 9 labeled (a) represents the susceptibility calculated from all

dx.doi.org/10.1021/ic502365h | Inorg. Chem. 2014, 53, 13174−13187

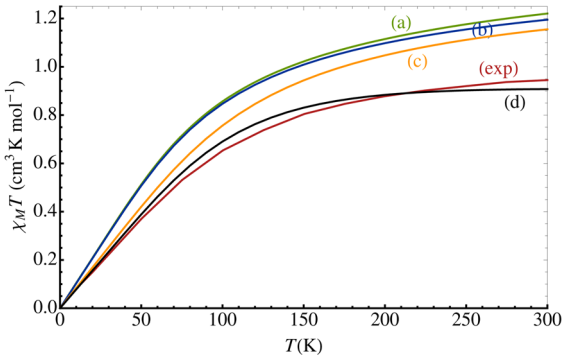

Figure 9. Magnetic susceptibility χT (cm^3 K mol^{-1}) as a function of T (K) calculated at the SCF-SO level for $(C_5Me_4H)_3UCl$ from eq 5: (a) sum over all calculated states, optimized structure; (b) optimized structure, using only the states listed in Table 2; (c) same as part b but with experimental structure; (d) experimental structure, using only the lowest A_1 and the lowest E state to calculate the susceptibility. The experimental (exp) curve was generated using data extracted from graphical material of ref 15.

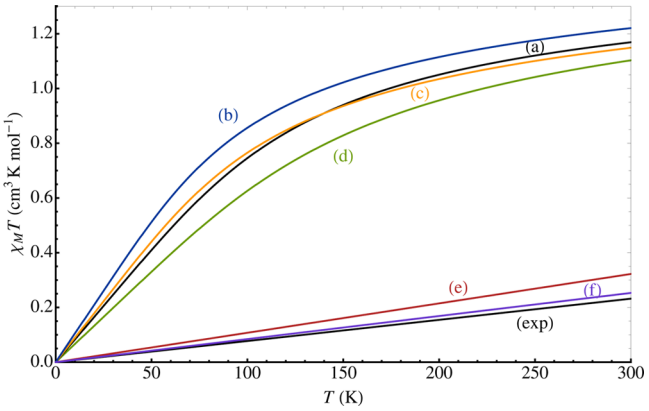

Figure 10. Magnetic susceptibility χT (cm^3 K mol^{-1}) as a function of T (K) obtained at the SCF-SO level for (a) X-ray structure of $(C_5Me_4H)_3UCl$, (b) optimized structure of $(C_5Me_4H)_3UCl$, (c) $(C_5H_5)_3UCl$, (d) $(C_5H_5)_3UCH_3$, (e) X-ray structure of $(C_5Me_4H)_3UNO$, (f) optimized structure of $(C_5Me_4H)_3UNO$ and (exp) experimental curve of $(C_5Me_4H)_3UNO$ generated using data extracted from graphical material of ref 15.

electronic states that were requested in the calculation, while curve (b) is based only on the low-energy states characterized in Table 2 deriving from the $^3H_4$ level of U^{4+}. There is close agreement between (a) and (b), with only minor differences appearing at higher T. The small contributions from the other calculated states is due to the considerable energy gap (over 3500 cm^{-1}) computed between the highest state deriving from the $^3H_4$ level and the lowest state deriving from the $^3F_2$ level. We can therefore assume that, within the investigated temperature range, electronic states that are even higher in energy than the ones used to generate curve a are negligible for the susceptibility, and likewise we assume that the calculated set of states gives converged susceptibilities for the other complexes.

The shape of the χT curve for $(C_5Me_4H)_3UCl$ is characteristic of $5f^2$ uranium complexes.[10] A qualitatively similar behavior is predicted for $(C_5H_5)_3UCH_3$ (Figure 10). Experimental susceptibilities are not available for this complex, but a very similar behavior has been observed for related Ar_3U-R complexes with organic ligands R such as C_4H_9, C_6H_5, and

Table 5. Temperature-Independent Paramagnetism (TIP) Range, TIP Magnetic Susceptibility, and Magnetic Susceptibility χT at 300 K for $(C_5Me_4H)_3UCl$, $(C_5H_5)_3UCl$, $(C_5H_5)_3UCH_3$, and $(C_5Me_4H)_3UNO$[a]

TIP range (K)	χ_{TIP} (cm^3 mol^{-1}) × 10^3	χT (cm^3 K mol^{-1})
$(C_5Me_4H)_3UCl$[b]		
0–60	8.515	1.174
(0–50)	(7.777)	(0.947)
$(C_5Me_4H)_3UCl$[c]		
0–40	10.440	1.220
(0–50)	(7.777)	(0.947)
$(C_5H_5)_3UCl$		
0–50	8.911	1.149
(0–90)	(6.6)	
$(C_5H_5)_3UCH_3$		
0–60	6.620	1.103
$(C_5Me_4H)_3UNO$[b]		
0–300	1.074	0.322
(0–300)	(0.777)	(0.232)
$(C_5Me_4H)_3UNO$[c]		
0–300	0.843	0.253
(0–300)	(0.777)	(0.232)

[a]Experimental data are given in parentheses where available. [b]Experimental geometry. [c]Optimized geometry.

trans-2-butenyl.[16] At low temperature, χT increases linearly with T. This is the TIP regime, as χ is constant and equal to the slope. The ground state of $(C_5Me_4H)_3UCl$ is nondegenerate, and consequently the first term on the right-hand side of eq 5 is zero for λ being the ground state itself. At low T, thermal population of excited states is negligible. The second term, with the energy denominators, is responsible for the TIP susceptibility. The calculated and experimental curves are in reasonably good agreement. The calculated TIP susceptibility χ_{TIP} is 8.52 and 10.44 (here and in the remainder of the text in units of 10^3 cm^3 mol^{-1}) for the experimental and optimized structure, respectively. The result for the X-ray structure is closer to the experimental χ_{TIP} of 7.78 but still overestimates somewhat. This may suggest that the energy of the first excited doublet state is calculated somewhat too low, as a too small energy denominator in the right-hand side of eq 5 would render the TIP susceptibility too large. Compared to the calculation with the experimental structure, the larger slope of χT calculated for the optimized geometry is indeed consistent with a lower energy of the first ^2E state for this geometry (Table 2). However, the magnetic transition moment matrix elements and contributions from excited states other than the lowest one also affect the magnitude of χ_{TIP}. Assuming accurate matrix elements and χ_{TIP} arising only from the first excited state, the initial slope of the experimental χT would require this ^2E state to be 268 cm^{-1} above the ground state. However, the aforementioned experimentally determined energy of 210 cm^{-1} is close to the SCF-SO energy calculated for the experimental structure. Hence, a combination of small errors in the magnetic moment matrix elements and possibly an underestimation of the energies of other excited states deriving from the $^3H_4$ level is likely responsible for the overestimation of the TIP susceptibility. If χT rises too fast in the TIP region this then also leads to an overestimation at higher T.

The susceptibility of $(C_5Me_4H)_3UCl$ becomes temperature dependent around ca. 70 K. In this regime, thermal population of degenerate excited states leads to nonzero contributions

dx.doi.org/10.1021/ic502365h | Inorg. Chem. 2014, 53, 13174–13187

from the first term on the right-hand side of eq 5, which has an intrinsic $1/T$ dependence from the factor β. In a two-state model with a nondegenerate ground state and a magnetic excited state, the high-T limit is characterized by (nearly) equal populations of the two states. Due to the sign change in the denominator of the second term in eq 5, the TIP contributions from the two states then cancel. In this case, the susceptibility χ would be proportional to $1/T$ from the excited state contribution to the first term, and consequently χT would become constant at high T. Obviously there are other excited states, but the behavior seen in the experimental curve approximately reflects this scenario. If we use only two states in the calculation of χT, the curve is in fact nearly horizontal around 300 K (curve d in Figure 9). The initial slope of curve (d) is still somewhat too high compared to experiment but closer than the calculations including all states. At 300 K the experimental χT is above curve (d) and has nonzero slope, showing that at this temperature the susceptibility affords contributions from other excited states. The overestimation of the calculated χT around 300 K can be attributed to an underestimation of the energies of these states, an overestimation of the relevant magnetic transition dipole matrix elements, a combination thereof, or solid-state packing effects affecting the experimental χT. The calculated χT curves for $(C_5Me_4H)_3UCl$ and $(C_5H_5)_3UCl$ are very similar. Slightly larger values for χ_{TIP} and χT at 300 K for the latter are consistent with a smaller energetic separation of the ground state and the lowest excited state.

In contrast with the other complexes, for $(C_5Me_4H)_3UNO$ the TIP regime extends to room temperature, in agreement with experiment. χ_{TIP} and χT at 300 K are in good agreement with experiment when using the optimized structure; for the experimental geometry the susceptibility is somewhat overestimated. This magnetic behavior is clearly a reflection of the strong stabilization of the ground state by the covalent interaction between the U center and NO, placing the first excited electronic state well above 3000 cm^{-1}. As seen in Figure 11, the TIP behavior of $(C_5Me_4H)_3NO$ does not arise from the magnetic coupling between the ground state and the first excited doublet E (see curve (c)), but is due principally to the magnetic coupling between the ground state and the second excited doublet E (see curve (b)).

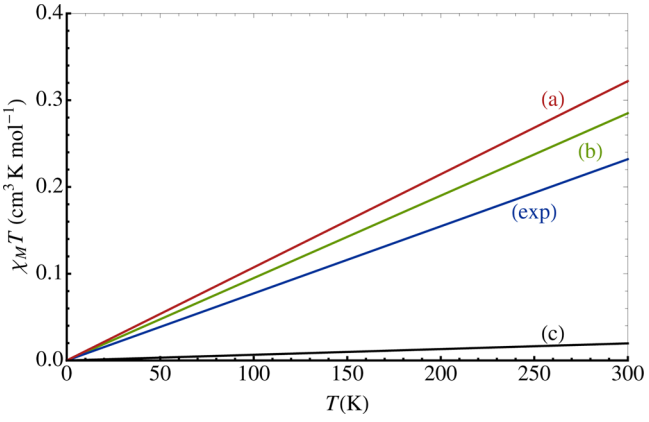

Figure 11. Magnetic susceptibility χT (cm^3 K mol^{-1}) as a function of T (K) calculated at the SCF-SO level for $(C_5Me_4H)_3UNO$ from eq 5: (a) sum over all calculated states, experimental structure; (b) experimental structure, using only the lowest A_1 and the two lowest E states to calculate the susceptibility; (c) experimental structure, using only the lowest A_1 and the lowest E state to calculate the susceptibility. The experimental (exp) curve was generated using data extracted from graphical material of ref 15.

4. SUMMARY

Magnetic properties and the low-energy part of the electronic spectra of $(C_5Me_4H)_3UCl$, $(C_5H_5)_3UCl$, $(C_5H_5)_3UCH_3$, and $(C_5Me_4H)_3UNO$ have been analyzed with the help of ab initio wave function calculations including SO coupling via state interaction of scalar relativistic CAS wave functions, and by DFT calculations. Chemical bonding, the nonbonding 5f orbitals, and the influence of SO coupling thereupon have been rationalized for selected states on the basis of the natural orbitals and their occupations. All complexes have nondegenerate ground states at the SO level. For the nitrosyl complex, the SF ground state is a closed-shell spin-singlet. For the other complexes the SF ground states are spin-triplets, with no orbital degeneracy for the chloride complexes and an orbital-doublet for the methyl complex (with an orbital-singlet very close in energy; in the SF DFT calculation the orbital singlet is the ground state). For the L = Cl, CH_3 complexes, the SF spin-triplet ground state wave functions contribute only between 12% and 40% to the SO ground state wave functions. The electronic structure of these complexes is therefore best analyzed by considering SO coupling first, and then consider the CF splitting of the $^3H_4$ term of U^{4+} from which the lowest-energy states of the complexes derive. Electronic g-factors for the low-energy states of these complexes calculated with a CF model and the $^3H_4$ term agree well with ab initio data. Differences can be attributed to admixtures of the $^1G_4$ term of U^{4+} in the ab initio wave functions which were not considered in the CF model. For $(C_5Me_4H)_3UNO$, SO coupling does not alter the fact that the ground state is nonmagnetic, but it has a noticeable influence on the U−NO π bond order. The excited states of $(C_5Me_4H)_3UNO$ are energetically well-separated from the ground state. The TIP of the system is dominated by the second excited state. The qualitative difference of the magnetic susceptibility as a function of temperature within 0 and 300 K is well-reproduced by the calculations. Quantitatively, the agreement of theory and experiment is reasonable.

■ ASSOCIATED CONTENT

Supporting Information

Additional data regarding the geometry optimizations, energies of electronic states at the PT2-SF and PT2-SO level, details about the procedure used for the extraction of the CF parameters, additional plots of orbitals and additional magnetic data, optimized structures corresponding to Table 1. This material is available free of charge via the Internet at http://pubs.acs.org.

■ AUTHOR INFORMATION

Corresponding Authors

*E-mail: boris.leguennic@univ-rennes1.fr.
*E-mail: jochena@buffalo.edu.

Notes

The authors declare no competing financial interest.

■ ACKNOWLEDGMENTS

F.G. and J.A. acknowledge support from the U.S. Department of Energy, Office of Basic Energy Sciences, Heavy Element Chemistry program, under Grant DE-FG02-09ER16066. We

acknowledge the Center for Computational Research (CCR) at the University at Buffalo for providing computational resources.

REFERENCES

(1) Lukens, W. W.; Edelstein, N. M.; Magnani, N.; Hayton, T. W.; Fortier, S.; Seaman, L. A. *J. Am. Chem. Soc.* **2013**, *135*, 10742−10754.
(2) Minasian, S. G.; Keith, J. M.; Batista, E. R.; Boland, K. S.; Clark, D. L.; Kozimor, S. A.; Martin, R. L.; Shuk, D. K.; Tyliszczak, T. *Chem. Sci.* **2014**, *5*, 351−359.
(3) Gagliardi, L.; Roos, B. O. *Nature* **2005**, *433*, 848−851.
(4) Layfield, R. A. *Organometallics* **2014**, *33*, 1084−1099.
(5) Rinehart, J. D.; Long, J. R. *Chem. Sci.* **2011**, *2*, 2078.
(6) Baldoví, J.; Cardona-Serra, S.; Clemente-Juan, J. M.; Coronado, E.; Gaita-Ariño, A. *Chem. Sci.* **2013**, *4*, 938−946.
(7) Bogani, L.; Wernsdorfer, W. *Nat. Mater.* **2008**, *7*, 179−186.
(8) Blagg, R. J.; Ungur, L.; Tuna, F.; Speak, J.; Comar, P.; Collison, D.; Wernsdorfer, W.; Mclnnes, E. J. L.; Chibotaru, L. F.; Winpenny, R. E. P. *Nat. Chem.* **2013**, *5*, 673−678.
(9) Thiele, S.; F, B.; Ballou, R.; Klyatskaya, S.; Rubben, M.; Wernsdorfer, W. *Science* **2014**, *344*, 1135−1138.
(10) Kindra, D. R.; Evans, W. J. *Chem. Rev.* **2014**, *114*, 8865−8882.
(11) Rinehart, J. D.; Long, J. R. *J. Am. Chem. Soc.* **2009**, *131*, 12558−12559.
(12) Meihaus, K. R.; Rinehart, J. D.; Long, J. R. *Inorg. Chem.* **2011**, *50*, 8484−8489.
(13) Mougel, V.; Chatelain, L.; Pécaut, J.; Caciuffo, R.; Colineau, E.; Griveau, J.-C.; Mazzanti, M. *Nat. Chem.* **2012**, *4*, 1011−1017.
(14) Castro-Rodríguez, I.; Meyer, K. *Chem. Commun.* **2006**, 1353−1368.
(15) Siladke, N. A.; Meihaus, K. R.; Ziller, J. W.; Fang, M.; Furche, F.; Long, J. R.; Evans, W. J. *J. Am. Chem. Soc.* **2012**, *134*, 1243−1249.
(16) Marks, T. J.; Seyam, A. M.; Kolb, J. R. *J. Am. Chem. Soc.* **1973**, *95*, 5529−5539.
(17) Eisenstein, J. C.; Pryce, M. H. L. *Proc. R. Soc. London, Ser. A* **1955**, *229*, 20−38.
(18) Kaltsoyannis, N. *Chem. Soc. Rev.* **2003**, *32*, 9−16.
(19) Kaltsoyannis, N.; Hay, P. J.; Li, J.; Blaudeau, J.-P.; Bursten, B. E. Theoretical Studies of the Electronic Structure of Compounds of the Actinide Elements. In *Chemistry of the Actinide and Transactinide Elements*; Katz, J. J., Morss, L. R., Edelstein, N., Fuger, J., Eds.; Springer: Dordrecht, The Netherlands, 2006.
(20) Autschbach, J.; Govind, N.; Atta-Fynn, R.; Bylaska, E. J.; Weare, J. H.; de Jong, W. A. Computational Tools for Predictive Modeling of Properties in Complex Actinide Systems. In *Computational Methods in Lanthanide and Actinide Chemistry*; Dolg, M., Ed.; Wiley: New York, in press.
(21) Case, D. A. *J. Chem. Phys.* **1985**, *83*, 5792.
(22) Arratia-Pérez, R.; Hernandez-Acevedo, L.; Malli, G. L. *J. Chem. Phys.* **2004**, *121*, 7743.
(23) Arratia-Pérez, R.; Malli, G. L. *J. Chem. Phys.* **2006**, *124*, 074321.
(24) Bolvin, H. *ChemPhysChem* **2006**, *7*, 1575−1589.
(25) Notter, F.-P.; Bolvin, H. *J. Chem. Phys.* **2009**, *130*, 184310−11.
(26) Verma, P.; Autschbach, J. *J. Chem. Theory Comput.* **2013**, *9*, 1052−1067.
(27) Verma, P.; Autschbach, J. *J. Chem. Theory Comput.* **2013**, *9*, 1932−1948.
(28) Autschbach, J.; Pritchard, B. *Theor. Chem. Acc.* **2011**, *129*, 453−466.
(29) Coutinho, J. T.; Antunes, M. A.; Pereira, L. C. J.; Bolvin, H.; Marçaloa, J.; Mazzanti, M.; Almeida, M. *Dalton Trans.* **2012**, *41*, 13568.
(30) Antunes, M. A.; Santos, I. C.; Bolvin, H.; Pereira, L. C. J.; Mazzanti, M.; Marçaloa, J.; Almeida, M. *Dalton Trans.* **2013**, *42*, 8861.
(31) Páez Hernández, D.; Bolvin, H. *J. Electron Spectrosc. Relat. Phenom.* **2014**, *194*, 74−80.
(32) Chibotaru, L. F.; Ungur, L. *J. Chem. Phys.* **2012**, *137*, 064112−22.
(33) Roos, B. O.; Taylor, P. R.; Siegbahn, P. E. M. *Chem. Phys.* **1980**, *48*, 157.
(34) Andersson, K.; Malmqvist, P.-A.; Roos, B. O.; Sadlej, A. J.; Wolinski, K. *J. Phys. Chem.* **1990**, *94*, 5483.
(35) Parr, R. G.; Yang, W. *Density Functional Theory of Atoms and Molecules*; Oxford University Press: New York, 1989.
(36) Gendron, F.; Páez-Hernández, D.; Notter, F.-P.; Pritchard, B.; Bolvin, H.; Autschbach, J. *Chem.—Eur. J.* **2014**, *20*, 7994−8011.
(37) Gendron, F.; Pritchard, B.; Bolvin, H.; Autschbach, J. *Inorg. Chem.* **2014**, *53*, 8577−8592.
(38) Karraker, D. G.; Stone, J. A. *Inorg. Chem.* **1972**, *11*, 1742−1746.
(39) Marks, T.; Seyam, A. M. *J. Am. Chem. Soc.* **1972**, *94*, 6545−6546.
(40) Amberger, H.-D.; Fischer, R. D.; Yünlü. *Organometallics* **1986**, *5*, 2109−2114.
(41) Amberger, H.-D.; Reddmann, H.; Edelstein, N. M. *Inorg. Chim. Acta* **1988**, *141*, 313−321.
(42) Bursten, B. E.; Rhodes, L. F.; Strittmatter, R. J. *J. Am. Chem. Soc.* **1989**, *111*, 2758−2766.
(43) Tatsumi, K.; Nakamura, A. *J. Organomet. Chem.* **1984**, *272*, 141−154.
(44) Gulino, A.; Cillberto, E.; Di Bella, S.; Fragala, I.; Seyam, A. M.; Marks, T. J. *Organometallics* **1992**, *11*, 3248−3257.
(45) te Velde, G.; Bickelhaupt, F. M.; Baerends, E. J.; van Gisbergen, S. J. A.; Fonseca Guerra, C.; Snijders, J. G.; Ziegler, T. *J. Comput. Chem.* **2001**, *22*, 931−967.
(46) Fonseca Guerra, C.; Snijders, J. G.; Te Velde, G.; Baerends, E. J. *Theor. Chem. Acc.* **1998**, *99*, 391.
(47) Baerends, E. J.; Ziegler, T.; Autschbach, J.; Bashford, D.; Bérces, A.; Bickelhaupt, F. M.; Bo, C.; Boerrigter, P. M.; Cavallo, L.; Chong, D. P.; Deng, L.; Dickson, R. M.; Ellis, D. E.; van Faassen, M.; Fan, L.; Fischer, T. H.; Fonseca Guerra, C.; Ghysels, A.; Giammona, A.; van Gisbergen, S. J. A.; Götz, A. W.; Groeneveld, J. A.; Gritsenko, O. V.; Grüning, M.; Gusarov, S.; Harris, F. E.; van den Hoek, P.; Jacob, C. R.; Jacobsen, H.; Jensen, L.; Kaminski, J. W.; van Kessel, G.; Kootstra, F.; Kovalenko, A.; Krykunov, M. V.; van Lenthe, E.; McCormack, D. A.; Michalak, A.; Mitoraj, M.; Neugebauer, J.; Nicu, V. P.; Noodleman, L.; Osinga, V. P.; Patchkovskii, S.; Philipsen, P. H. T.; Post, D.; Pye, C. C.; Ravenek, W.; Rodríguez, J. I.; Ros, P.; Schipper, P. R. T.; Schreckenbach, G.; Seldenthuis, J. S.; Seth, M.; Snijders, J. G.; Solà, M.; Swart, M.; Swerhone, D.; te Velde, G.; Vernooijs, P.; Versluis, L.; Visscher, L.; Visser, O.; Wang, F.; Wesolowski, T. A.; van Wezenbeek, E. M.; Wiesenekker, G.; Wolff, S. K.; Woo, T. K.; Yakovlev, A. L. *Amsterdam Density Functional*; SCM, Theoretical Chemistry, Vrije Universiteit: Amsterdam, The Netherlands, http://www.scm.com.
(48) van Lenthe, E.; Baerends, E. J.; Snijders, J. G. *J. Chem. Phys.* **1993**, *99*, 4597−4610.
(49) Becke, A. D. *J. Chem. Phys.* **1993**, *98*, 5648−5652.
(50) Aquilante, F.; De Vico, L.; Ferré, N.; Ghigo, G.; Malmqvist, P.; Neogrády, P.; Pedersen, T. B.; Pitoňák, M.; Reiher, M.; Roos, B. O.; Serrano-Andrés, L.; Urban, M.; Veryazov, V.; Lindh, R. *J. Comput. Chem.* **2010**, *31*, 224−247.
(51) Wolf, A.; Reiher, M.; Hess, B. A. *J. Chem. Phys.* **2002**, *117*, 9215−9226.
(52) Malmqvist, P.-A.; Roos, B. O.; Schimmelpfennig, B. *Chem. Phys. Lett.* **2002**, *357*, 230.
(53) Pritchard, B. *Calculation of Magnetic Properties of Paramagnetic Molecules*. Thesis, University at Buffalo, State University of New York, 2014.
(54) Cloke, F. G. N.; Hawkes, S. A.; Hitchcock, P. B.; Scott, P. *Organometallics* **1994**, *13*, 2895−2897.
(55) Wong, C. H.; Yen, T.-M.; Lee, T.-Y. *Acta Crystallogr., Sect. C* **1965**, *18*, 340−345.
(56) Elkechai, A.; Boucekkine, A.; Belkhiri, L.; Amarouche, M.; Clappe, C.; Hauchard, D.; Ephritikhine, M. *Dalton Trans.* **2009**, 2843−2849.
(57) Elkechai, A.; Mani, Y.; Boucekkine, A.; Ephritikhine, M. *Inorg. Chem.* **2012**, *51*, 6943−6952.
(58) Strittmatter, R. J.; Bursten, B. E. *J. Am. Chem. Soc.* **1991**, *113*, 552−559.

(59) Reynolds, L. T.; Wilkinson, G. *J. Inorg. Nucl. Chem.* **1956**, *2*, 246−253.
(60) Craw, J. S.; Vincent, M. A.; Hillier, I. H. *J. Phys. Chem.* **1995**, *99*, 10181−10185.
(61) Hay, P. J.; Martin, R. L.; Schreckenbach, G. *J. Phys. Chem. A* **2000**, *104*, 6259−6270.
(62) da Cunha, T. T.; Jung, J.; Boulon, M.-E.; Campo, G.; Pointillart, F.; Pereira, C. L. M.; Le Guennic, B.; Cador, O.; Bernot, K.; Pineider, F.; Golhen, S.; Ouahab, L. *J. Am. Chem. Soc.* **2013**, *135*, 16332−16335.
(63) Jung, J.; da Cunha, T. T.; Le Guennic, B.; Pointillart, F.; Pereira, C. L. M.; Luzon, J.; Golhen, S.; Cador, O.; Maury, O.; Ouahab, L. *Eur. J. Inorg. Chem.* **2014**, 3888−3894.
(64) Ruud, K.; Åstrand, P.-O.; Taylor, P. R. *J. Chem. Phys.* **2000**, *112*, 2668−2683.
(65) Ruud, K.; Taylor, P. R.; Jaszunski, M. *J. Phys. Chem. A* **2000**, *104*, 168−169.
(66) Krykunov, M.; Autschbach, J. *J. Chem. Phys.* **2007**, *126*, 024101−12.
(67) Cybulski, S. M.; Bishop, D. M. *J. Chem. Phys.* **1994**, *100*, 2019−2026.
(68) Stevens, K. W. H. *Proc. Phys. Soc., London, Sect. A* **1952**, *65*, 209.
(69) Judd, B. R. *Proc. Phys. Soc., London, Sect. A* **1955**, *227*, 552.
(70) Abragam, A.; Bleaney, B. *Electron Paramagnetic Resonance of Transition Ions*; Clarendon Press: Oxford, 1970.
(71) Judd, B. R. *Proc. Phys. Soc., London, Sect. A* **1955**, *232*, 458.
(72) Atherton, N. M. *Principles of Electron Spin Resonance*; Ellis Horwood Series in Physical Chemistry; Prentice Hall: New York, 1993.
(73) Wang, X.; Andrews, L.; Vlaisavljevich, B.; Gagliardi, L. *Inorg. Chem.* **2011**, *50*, 3826−3831.
(74) Gagliardi, L.; Roos, B. O. *Inorg. Chem.* **2003**, *42*, 1599−1603.
(75) Brogden, D. W.; Turov, Y.; Nippe, M.; Li Manni, G.; Hillard, E. A.; Clérac, R.; Gagliardi, L.; Berry, J. F. *Inorg. Chem.* **2014**, *53*, 4777−4790.
(76) Brynda, M.; Gagliardi, L.; Roos, B. O. *Chem. Phys. Lett.* **2009**, *471*, 1−10.
(77) Roos, B. O.; Borin, A. C.; Gagliardi, L. *Angew. Chem., Int. Ed.* **2007**, *46*, 1469−1472.
(78) Vancoillie, S.; Neese, F.; Rulisek, L.; Pierloot, K. *J. Phys. Chem. A* **2009**, *113*, 6149−6157.